RSC Advances

PAPER

View Article Online
View Journal | View Issue



Cite this: *RSC Adv.*, 2016, **6**, 69301

# Photolysis and photocatalytic decomposition of sulfamethazine antibiotics in an aqueous solution with $TiO_2$†

Tai-Wei Tzeng,[a] Shan-Li Wang,[b] Chiing-Chang Chen,[c] Chen-Chung Tan,[a] Yu-Ting Liu,[a] Tsan-Yao Chen,[d] Yu-Min Tzou,*[a] C.C. Chen[e] and J. T. Hung*[f]

Photo-decomposition of sulfamethazine (SMT) involves photolytic and photo-catalytic reactions, which occur simultaneously. The relative contributions of these two reactions to the overall SMT photo-decompositions by $TiO_2$ and the intermediates of SMT photo-decompositions were systematically examined with the effects of $TiO_2$ loading, and the pH and the initial SMT concentrations in the solutions. The apparent rate constants of SMT photo-decomposition reactions, which were well described by the pseudo-first-order kinetic model, ranged from 0.24 to 1.61 $h^{-1}$. The overall photo-decomposition efficiencies of 0.072 mM SMT were the highest at pH 5.5 with 0.5 g $L^{-1}$ $TiO_2$ due to the adsorption-induced photocatalytic decomposition of SMT on $TiO_2$. However, the SMT photolysis occurred more rapidly at pH 10. Two reactive species of holes and hydroxyl radicals concurrently participated in the photocatalytic decomposition of SMT, and the latter dominated the oxidative reactions of SMT on $TiO_2$. Eight intermediates of SMT photo-decomposition were determined using LC-MS. Their time-dependent distributions indicated that the photo-decomposition of SMT was triggered by hydroxylation on aniline and dimethylpyrimidinyl moieties, followed by the cleavage of the S–N bond of SMT. Our results illustrated that the intermediates with dimethylpyrimidinyl groups possess strong resistance to photo-decomposition and played a determinant role in the photo-decomposition of SMT.

Received 24th May 2016
Accepted 11th July 2016

DOI: 10.1039/c6ra13435a

www.rsc.org/advances



## 1. Introduction

The presence of pharmaceuticals and personal care products (PPCPs) has received great scientific concern due to their potential impacts on the normal functionalities of ecosystems.[1] Veterinary drugs, *e.g.*, sulfonamide antibiotics, a typical class of PPCPs, were commonly applied to livestock animals for therapeutic purposes, and these compounds have been widely distributed in the environment because of unintentional or intentional discharges during agricultural activities. For instance, sulfamethazine (SMT), a major sulfonamide antibiotic with a functional group of $-SO_2NH_2-$, is commonly used to control infectious diseases and facilitate animal growth.[2,3] Because veterinary drugs cannot be completely metabolized after their uptake by animals, up to 90% of SMT is excreted *via* feces and urine and ends up in animal manures.[4,5] The SMT-containing manures, either in fresh condition or after being composted, are frequently applied as a fertilizer. This unstoppable campaign caused by long-term agricultural activities has led to the widespread presence of SMT in farmlands. Subsequently, the SMT may be relocated through surface runoff/leaching into surface and ground water, drinking waters, or eventually the entire ecosystems.[6,7] In addition, SMT may be accumulated in soils and sediments or be spread out through the food chain, leading to the development of antibiotic resistances.[8–10] Consequently, a decrease or loss in the treatment potency of antibiotics against human diseases may result in a huge disaster in public health. Therefore, it is important and necessary to eliminate SMT residues in the environment.

SMT exhibits a semi-resistance to biological degradation, and thus, the traditional sewage treatment systems with

[a]*Department of Soil and Environmental Sciences, National Chung Hsing University, 250 Kuo-Kuang Rd., Taichung, 40227, Taiwan, Republic Of China. E-mail: ymtzou@dragon.nchu.edu.tw; Fax: +886-4-22855167; Tel: +886-4-22840373 ext. 4206*

[b]*Department of Agricultural Chemistry, National Taiwan University, Taipei, Taiwan, Republic Of China*

[c]*Department of Science Education and Application, National Taichung University of Education, Taichung, Taiwan, Republic Of China*

[d]*Department of Engineering and System Science, National Tsing Hua University, Hsinchu, Taiwan, Republic Of China*

[e]*Department of Life Science, National Taiwan Normal University, Taipei 116, Taiwan, ROC*

[f]*Department of Horticulture and Landscape Architecture, National Taitung Junior College, Taitung 95045, Taiwan*

† Electronic supplementary information (ESI) available. See DOI: 10.1039/c6ra13435a

a biological process may be less effective decreasing the concentrations of SMT discharges to a level with low or no environmental risk.[11,12] Advanced oxidation techniques (AOPs), such as electro-Fenton,[13,14] sonolysis,[15] and photo-Fenton process,[16] have been employed to remove the antibiotics or metabolites of SMT. However, the productions of extra wastes, *e.g.*, Fe – containing sludge, substantially increase the operation cost. Heterogeneous photocatalysis, one of the typical AOPs, using the stable and low toxic catalysts such as $TiO_2$ is a potential cost-effective alternative because the $TiO_2$ catalysts can provide high efficiency of converting photo- to chemical-energy and promote photo-decomposition of antibiotics[17,18] and organic pollutants.[19–22] As $TiO_2$ particles are irradiated by the photons with energy greater than the band gap of the semiconductor, the electrons ($e^-$) are ejected from the valence band (VB) to the conduction band (CB). This electronic movement generates a photovoltage and creates a charge separation, leading to the productions of an electron deficiency or positively charged hole ($h^+$) in the VB and an enrichment of negative charge, $e^-$, in the CB. The redox couples of $e^-/h^+$ on the surfaces of $TiO_2$ then participate in the redox reactions with water/oxygen or contaminants. The VB hole can act as a strong oxidizer or promote the formation of strong oxidants, *e.g.*, OH radicals[23] and the CB electrons can serve as a reductant for the redox reactions. The productions of hole ($h^+$) and electron ($e^-$) on $TiO_2$ upon absorption of light energy are described in eqn (1), and the hydroxyl radical productions associated with oxygen reductions are expressed in eqn (2) and (3), respectively.

$$TiO_2 \xrightarrow{h\nu} e^- + h^+ \quad (1)$$

$$TiO_2(h^+) + H_2O/OH^- \rightarrow TiO_2(h^+) - H_2O/OH^- \rightarrow TiO_2 + {}^{\bullet}OH \quad (2)$$

$$TiO_2(e^-) + O_2 \rightarrow TiO_2 + O_2^{-\bullet} \quad (3)$$

The possible reactions of forming peroxylated intermediates and degraded products upon decomposition of the organic compounds (electron donors, $Red_{org}$) by OH radicals and superoxide radicals ($O_2^{-\bullet}$) are described in eqn (4), and (5), respectively.[24]

$$^{\bullet}OH + Red_{org} \rightarrow Ox''_{org} \quad (4)$$

$$O_2^{-\bullet} + Red_{org} \rightarrow \text{peroxylated intermediates} \rightarrow \text{degraded products} \quad (5)$$

On the other hand, if the organic compound exhibits a more negative redox potential than that of hole, the organic can be oxidized by the hole, giving a cation radical of the specific organic (eqn (6)).

$$TiO_2(h^+) + S \rightarrow TiO_2 + S^{\bullet+} \rightarrow \text{product} \quad (6)$$

The photocatalytic decompositions of organic pollutants such as sulfa-containing drugs, including kinetics and mechanisms, had been previously investigated on $TiO_2$. For instance, Hu *et al.*[25] studied the photo-oxidation of sulfamethoxazole using $TiO_2$ as a photocatalyst under UV-A irradiation. The authors found that even if the amounts of sulfamethoxazole adsorbed on the $TiO_2$ surfaces were very low, rapid photo-oxidization of sulfamethoxazole was still observed on $TiO_2$. Jiao *et al.*[26] reported that tetracycline antibiotic could proceed a self-photolytic reaction, which was highly pH-dependent and controlled partially the antibiotic concentrations in the environments.[27,28] Although Calza *et al.*[29] and Beltrán *et al.*[20] had addressed the photo-decomposition of sulfonamide antibiotics on $TiO_2$, the proportions of surface adsorption and photolytic of SMT involved in the photo-induced redox reactions as influenced by pH remained unknown.

In this study, the photo-decomposition pathways of SMT with $TiO_2$ were deduced in terms of the formation of intermediates, which were analyzed by electrospray ionization mass spectrometry in both the positive ($ESI^+$) and negative ($ESI^-$) ion modes, and the fragment ion patterns were obtained by total ion chromatogram (TIC). The differences in the photodecomposition products or intermediates of SMT identified using these two modes were examined and compared. Because a large number of small molecules are easily ionized by the $ESI^-$ rather than that by the $ESI^+$, both modes were simultaneously applied in the study to identify the photo-induced products of SMT in the same system.[30,31] Effects of initial concentrations of SMT, $TiO_2$ loadings, pH, and photo-induced radicals on SMT decompositions were also investigated. Thus, the major goals of this study were to (1) clarify the contributions of adsorption and photolytic reactions to the photocatalytic decomposition of SMT in the presence of $TiO_2$, (2) characterize the stable reaction intermediates and products, and (3) propose the dominant photo-decomposition pathways of SMT.

## 2. Materials and methods

### 2.1 Chemicals

$TiO_2$ (Degussa P25) was purchased from Sigma-Aldrich and used as received. The crystal form contents, surface area, and crystalline size of $TiO_2$ Degussa P25 were 75% anatase and 25% rutile, 50 ± 1.0 $m^2\ g^{-1}$, and about 20 nm with non-porous structures, respectively.[32] The SMT antibiotic ($C_{12}H_{14}N_4O_2S$) with a purity of 99% and molecular weight of 278.34 g $mol^{-1}$ was also purchased from Sigma-Aldrich and used without further purification. The stock solution of 100 mg $L^{-1}$ SMT was prepared by dissolving 0.1 g of SMT in 1 L de-ionized water and stored in the dark at 4 °C. Because the concentration of SMT was subject to change with pH, especially at high pH, a $NaH_2BO_3$ buffer solution was prepared by dissolving 5.1 g $H_3BO_3$ and 2 g NaOH in 1 L de-ionized water at a pH of 10 to maintain the solution pH during SMT measurement.

### 2.2 Photocatalytic reactor

All experiments, including adsorption, photolysis, and photocatalysis, were performed in a chamber with eight UV lamps (20 watts for each lamp) (GL20, Sankyo Denki, Japan) with an UV-A intensity of 20.8 μW $cm^{-2}$ detected by a OPAS UV-A spotter (SN: 811013T, USA). A 500 mL quartz double-wall water jacked reactor, which was connected to a circulating waterbath to

 

maintain a constant temperature in the reactor, was placed in the center of the chamber surrounded by the lamps. The lamps were switched on for at least 5–10 min to obtain a stable emission prior to conducting the experiments of photo-reactions. One end of a plastic tube was inserted into the reactor, and the sample solution was extracted using a syringe connected to the other end of the tube. Before each sample collection, the tube was pumped and purged several time to ensure the sample was not contaminated by the residual suspensions in the tube.

### 2.3 Experimental procedures

**2.3.1 Adsorption.** The adsorption of SMT on $TiO_2$ was carried out using a batch method in the dark. The initial SMT concentrations varying from 0.036 to 0.162 mM were freshly prepared from a 100 mg $L^{-1}$ stock solution. The solution of each SMT concentration was then added into a 500 mL quartz beaker containing $TiO_2$ with a dosage of 0.5, 1.0, or 2.0 g $L^{-1}$, respectively. The pH values of the suspensions were adjusted to 3, 5.5, and 10 using 1.0 M HCl or NaOH and the suspensions were stirred continuously for 24 h. Right after the sample was extracted and filtrated, SMT in the filtrate was measured colorimetrically (details please see below). The differences in SMT concentrations before and after the reactions were attributed to adsorption.

**2.3.2 Photo-decomposition of SMT.** Occurrence of the self-photolysis of SMT was first evaluated in the absence of $TiO_2$ under UV irradiation at pH 3–10. The photo-decomposition of SMT was started after 0.036, 0.072, or 0.162 mM SMT was reacted with 0.1–2.0 g $L^{-1}$ $TiO_2$ at pH 3–10 in the dark for 1 h. The overall photo-decomposition of SMT in the presence of $TiO_2$ involved both photo-catalytic decomposition of SMT (PCDS) on $TiO_2$ and photolysis of SMT. Thus, the contributions of PCDS to SMT decomposition could be approximately estimated by subtracting the photolysis of SMT from the overall SMT photo-decomposition. During the photo-decomposition processes of SMT, the full-UV scanning spectra, including the decomposition intermediates of SMT, were obtained by a HPLC coupled with mass spectra, and the dissolved carbon contents were determined by a total organic carbon (TOC) analyzer (details please see below). In addition, the contributions of hydroxyl radicals ($^{\bullet}OH$) and hole ($h^+$) to photo-catalytic decomposition of SMT were also examined by adding two radical scavengers of isopropanol (ISP) and sodium iodide (NaI) to capture hydroxyl radicals ($^{\bullet}OH$) and hole ($h^+$), respectively.[24]

### 2.4 Analytical methods

**2.4.1 SMT concentrations.** The SMT-containing filtrates obtained after the samples were periodically extracted using a syringe and passed through a 0.2 μm pore-sized cellulose acetate membrane filter (Advantec). Two millimeters of $NaH_2BO_3$ buffer solution (pH = 10) were added into a filtrate of 8 mL prior to the determination of SMT concentrations to avoid the pH-dependent changes in SMT species during spectroscopic analyses.[33–35] The changes in SMT concentrations during the adsorption and photo-decomposition processes were detected using a UV-visible spectrophotometer (Spectro UV-2550, Labomed, USA) at a wavelength of 262 nm.

**2.4.2 Dissolved organic carbon and anions.** The extent of photo-decomposition of SMT was examined by measuring the dissolved organic carbon (DOC) using a TOC analyzer (Analyticjena multi N/C 2100, Germany). The inorganic anions contents in the solution, *i.e.*, $NO_2^-$, $NO_3^-$, and $SO_4^{2-}$, were quantified by an ion chromatography (883 basic IC plus, Metrohm; Swissmade). An anion exchange column (Metrosep A Supp5) was used with 3 mM $Na_2CO_3$ and 1 mM $NaHCO_3$ as mobile phase at a flow rate of 0.7 mL $min^{-1}$.[36,37] The $NH_4^+$ concentration was measured using a cation exchange column (Metrosep C 4) with an eluent containing 0.7 mM dipicolinic acid and 1.7 mM nitric acid at a flow rate of 0.9 mL $min^{-1}$.

**2.4.3 Intermediates of SMT photo-decomposition.** The full-scan UV spectra of a high performance liquid chromatography (Waters 1525 Binary HPLC) equipped with a photodiode array detector (Model code 2998, USA) were used to determine the intermediates of SMT photo-decomposition. A C18 reverse phase column (Atlantis, Waters) was applied to separate the intermediates in 100 μL filtrate using a gradient method with two mobile phases at a flow rate of 1.0 mL $min^{-1}$.[38] Briefly, the percentage of mobile phase A (de-ionized water) was maintained at 95% for the first 30 min, followed by increasing linearly the percentage of mobile phase B (acetonitrile) to 100% within 20 min and to 5% for the next 10 min. The intermediates were identified by the mass spectrometry (Waters 3100, USA) with an electrospray interface (ESI) which was operated in both positive and negative ionization modes. The full-UV absorbing spectra of the intermediates were detected by the photodiode array detector which was connected behind ESI.

### 2.5 Kinetics of SMT decomposition

The Langmuir–Hinshelwood (L–H) kinetic model was applied to analyze the photo-decomposition of SMT (eqn (7)):[39]

$$r_0 = \left(-\frac{dC}{dt}\right)_0 = \frac{k_r K_{ad} C_0}{1 + K_{ad} C_0} \quad (7)$$

where, $C_0$ (mM) and $K_{ad}$ (L $mmol^{-1}$) represent the initial concentration of SMT and the reactant adsorption constant of SMT on $TiO_2$ surfaces, respectively. The $k_r$ (mM $h^{-1}$) is the intrinsic reaction rate constant related to the catalyst mass and efficient photon flow.[40]

When the SMT concentration is very low (*i.e.* $K_{ad}C_0 \ll 1$), The L–H kinetic model can be simplifies to a pseudo-first-order (PFO) model (eqn (8)).[21,25]

$$-\ln\left(\frac{C}{C_0}\right) = k_{app} \times t \quad (8)$$

where, $C_0$ (mM) and $C$ (mM) are the initial concentration and the concentration of SMT at reaction time $t$, respectively. The $k_{app}$ ($h^{-1}$) value, the slope of PFO linear curve represents an apparent PFO reaction rate constant.

The contributions of PCDS on $TiO_2$ to the overall SMT photo-decomposition were calculated by deducting the amount of SMT self-photolysis from the overall photo-decomposition of

SMT. Thus, the PFO rate constant of PCDS on $TiO_2$ could be obtained (eqn (9)).

$$-\ln\left(\frac{C_0 - (C_{UV} - C_{overall})}{C_0}\right) = k_{app,TiO_2} \times t \quad (9)$$

where, $C_{UV}$ and $C_{overall}$ are the concentrations of photolytic and overall photo-decomposition reactions of SMT at time $t$, respectively. The $k_{app,TiO_2}$ ($h^{-1}$) represents the PFO reaction rate constant of PCDS on $TiO_2$.

# 3. Results and discussion

## 3.1 Adsorption of SMT on $TiO_2$

The SMT adsorption on $TiO_2$ was carried out for 24 h in the absence of light at pH 3, 5.5, and 10. The results showed that SMT adsorption was low at each tested pH; the highest adsorption amount of SMT (*i.e.*, 0.54 mmol $kg^{-1}$) occurred at pH 5.5 (Fig. 1), attributed to a favorable electrostatic interaction between SMT and $TiO_2$ at the specific pH. Depending on the solution pH, SMT can be protonated and deprotonated, forming charged species of $SMT^+$ and $SMT^-$, respectively, or be converted to form the neutral species of $SMT^0$ (Fig. 1). On the other hand, the $TiO_2$ adsorbent has a point of zero charge at 6.5,[41] and thus, the surfaces of $TiO_2$ exhibit a pH-dependent charge properties of SMT, forming $TiOH_2^+$, TiOH, or $TiO^-$.[42] At pH 3 and 10, both SMT and $TiO_2$ bore the same charges, leading to an unfavorable (repulsive) condition for SMT adsorption. At pH 5.5, the neutral form of $SMT^0$ dominated in the solution, and thus, the electrostatic repulsion between neutral SMT and positively charged $TiO_2$ was lower. In addition, the conversion of $SMT^0$ to relative stable zwitterions ($SMT^{\pm}$) in the presence of positively charged $TiO_2$ (ref. 43) may facilitate SMT adsorption on $TiO_2$ through the polarized $-SO_2N-$ group of $SMT^{\pm}$. However, the $SMT^{\pm}$ comprises less than 0.2% of $SMT^0$ in an aqueous solution.[44] Therefore, the enhancement of SMT adsorption due to the changes in SMT species induced by the charged surfaces of $TiO_2$ was relatively insignificant.

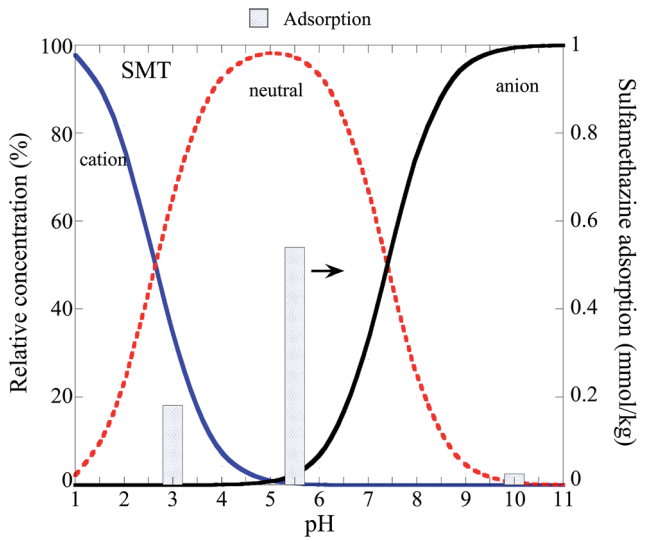


Fig. 1 The pH-dependent speciation of sulfamethazine (SMT) and the adsorption amount of SMT. Adsorption experiment was conducted in a system with an initial SMT concentration of 0.072 mM and 0.5 g $L^{-1}$ $TiO_2$.

## 3.2 Photolysis and photocatalytic degradation of SMT

The occurrences of photolysis of SMT were first estimated under UV irradiation in the absence of $TiO_2$. The changes of SMT concentrations upon photolysis of 0.072 mM SMT at three pH values, presented in Fig. 2a, showed that photolysis of SMT was pH-dependent and the maximum photolytic reactions of SMT occurred at pH 10 with a PFO rate constant of 0.58 $h^{-1}$ (Fig. 2a, inserted and Table 1). About 61, 22, and 15% of SMT

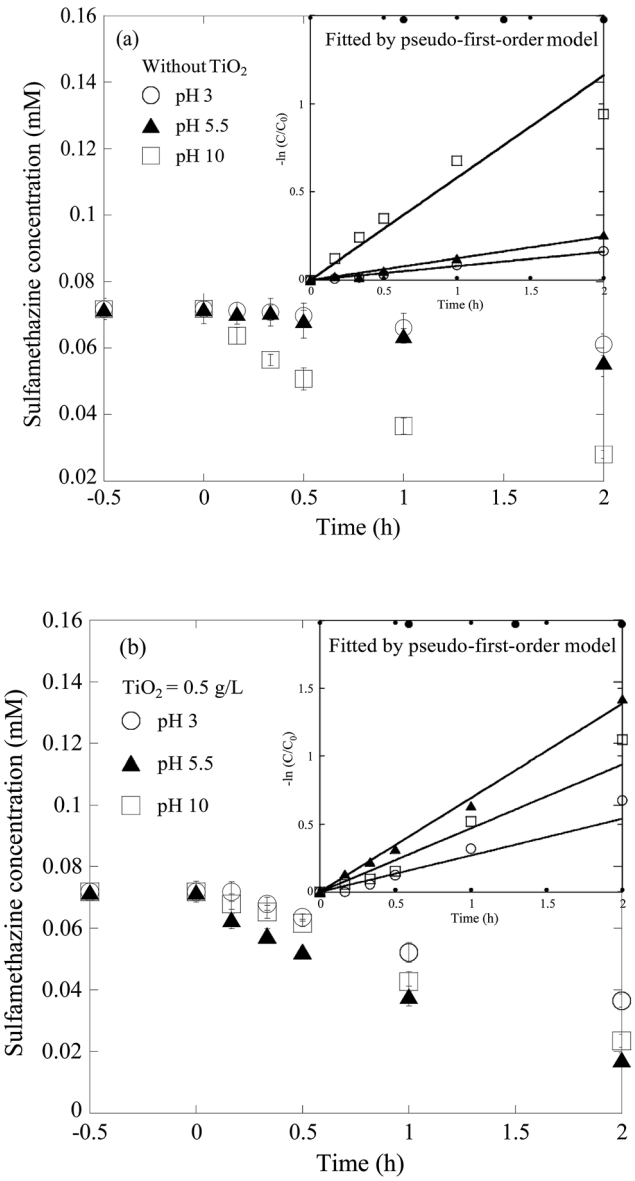


Fig. 2 The influences of the solution pHs on an initial concentration 0.072 mM sulfamethazine (a) photolysis and (b) photo-decomposition. The self-photolytic reaction of sulfamethazine (SMT) in the absence of $TiO_2$. The inset was the simulation results of photolytic and photo-decomposition on SMT using the PFO model.

Table 1 Pseudo-first-order (PFO) rate constants of sulfamethazine (SMT) self-photolytic reactions, photo-catalytic decomposition of SMT (PCDS) on 0.5 g $L^{-1}$ $TiO_2$, and the overall photo-decomposition of SMT at pH 3, 5.5, and 10. The initial SMT concentration was 0.072 mM

| Pseudo-first-order parameters | | | | | | |
|---|---|---|---|---|---|---|
| | Self-photolysis | | PCDS on $TiO_2$ | | Overall photo-decomposition | |
| pH | $k_{app}$[a] ($h^{-1}$) | $r^2$ | $k_{app,TiO_2}$ ($h^{-1}$) | $r^2$ | $k_{app}$ ($h^{-1}$) | $r^2$ |
| 3 | 0.06 | 0.98 | 0.21 | 0.99 | 0.27 | 0.96 |
| 5.5 | 0.12 | 0.99 | 0.41 | 0.98 | 0.69 | 0.99 |
| 10 | 0.58 | 0.98 | 0.025 | 0.83 | 0.47 | 0.99 |

[a] $k_{app}$ represented the rate constant of pseudo-first-order (PFO) model.

disappeared at pH of 10, 5.5, and 3, respectively, after 2 h reactions under illumination. The results may be attributed to the differences in the light sensitivity of the three SMT species (*i.e.*, $SMT^+$, $SMT^0$, and $SMT^-$). Baeza and Knappe[45] reported that the anionic form of SMT exhibited a higher molar absorption coefficient than the cationic and neutral forms of SMT. Therefore, we presumed that, at pH 10, the dominant anionic form of SMT may absorb more photons and lead to a greater photolysis of SMT. In addition, Challis *et al.*[46] found that the photochemical activity of sulfonamide antibiotics was related to their $pK_{a_2}$ values, determined mainly by the numbers of $CH_3$ groups on the heterocyclic ring of sulfonamide antibiotic. While being attached, $CH_3$ group could offset the electron withdrawal by the two N atoms in the heterocyclic substituents of sulfonamide antibiotics, resulting in a decrease in the proton-donating ability of NH (or $NH_2$) and $pK_{a_2}$ value. These authors further demonstrated that the sulfonamide with a lower $pK_{a_2}$ exhibited a greater photolytic degradation efficiency of sulfonamide at high pH.[46] Because the SMT, bearing two $CH_3$ groups on the heterocyclic ring, has a lower $pK_{a_2}$ as compared to that of sulfonamide, the SMT was expected more susceptive to the photo-energy. Thus, a rapid photolysis of SMT occurred, particularly at a higher pH, at which $SMT^-$ was the dominant species of SMT (Fig. 2a). A similar result reported in ref. 47 showed that the $SMT^-$ exhibited a higher degradation efficiency upon exposure to a simulated solar radiation. Because SMT can proceed a self-photolytic reaction, to evaluate precisely the role of $TiO_2$ for heterogeneous catalysis of SMT decomposition, photolytic reactions of SMT must be excluded from the overall photo-decomposition of SMT.

Influences of the solution pH (3, 5.5, and 10), SMT initial concentrations (0.036, 0.072, and 0.162 mM), and $TiO_2$ loadings (0.1, 0.5, and 2.0 g $L^{-1}$) on photo-decomposition of SMT were investigated. In the system with $TiO_2$, approximately 76% removal efficiency of SMT was observed after the system was exposed to the light for 2 h at a pH of 5.5. About 67% of SMT was photo-decomposed at pH 10 and the decomposition efficiency of SMT was the lowest at pH 3 (49%) after the same reaction time, *i.e.*, 2 h (Fig. 2b). Indifferent to the reaction pH, the overall SMT photo-decomposition followed the PFO model, and the apparent PFO reaction rate constant ($k_{app}$) values were 0.69, 0.47, and 0.27 $h^{-1}$ at pH 5.5, 10, and 3.0, respectively (Table 1). At pH 10, even if the photolysis of SMT proceeded rapidly with a $k_{app}$ of 0.58 $h^{-1}$, no discernible PCDS were observed (Fig. S1† and Table 1). Thus, the overall photo-decomposition rate of SMT was lower at pH 10 than that at pH 5.5 (Table 1) at which $TiO_2$ exhibited a higher adsorption capacity and photo-catalytic rate (Fig. S1 and S2†).

In the $TiO_2$ system, the SMT photo-decomposition involved two reactions of SMT self-photolysis and PCDS (*i.e.*, photo-catalytic decomposition of SMT) on the $TiO_2$ surfaces. While the contributions of photolytic decomposition of SMT to the overall SMT photo-decomposition was deducted, the PCDS on the $TiO_2$ surfaces could be obtained (Fig. S1†). Although photolytic decomposition of SMT exhibited the highest efficiency at pH 10 (Fig. 2a and S2†), the contributions of PCDS on $TiO_2$ to the overall SMT photo-decomposition was the lowest (Fig. S2†). At pH 10, the low efficiency of PCDS (Fig. S2†) was probably attributed to the low adsorption of SMT on $TiO_2$ (Fig. 1) due to electrostatic repulsion (negative) between these the adsorbent and adsorbate. In contrast, neutral SMT exhibited a higher affinity to the surfaces of $TiO_2$ at pH 5.5, and thus, a significant amount of SMT adsorption was observed (Fig. S2†). The reaction rate ($k_{app,TiO_2}$) of PCDS on $TiO_2$ also exhibited a maximum value at pH 5.5 (Table 1). According to the reports of ref. 48–50, the heterogeneous photocatalytic reaction on the surfaces of $TiO_2$ involved five steps: (1) generation of the electron–hole pairs on $TiO_2$ by absorbing light energy higher than 3.2 eV; (2) separation of the photo-generated electrons and holes; (3) productions of OH radicals or superoxide radicals when the holes and electrons migrated to the surfaces of $TiO_2$ and interacted with the adsorbed $H_2O$/hydroxyl groups and dissolved oxygen, respectively (eqn (2) and (3)); (4) occurrences of oxidative reactions in a solution with electron donors by OH radicals (eqn (4)), superoxide radicals ($O_2^{-\bullet}$) (eqn (5)), or photo-generated holes of $TiO_2$ (eqn (6)); and (5) desorption of the reaction products and reconstruction of the $TiO_2$ surfaces. The higher efficiency for catalytic decomposition of SMT on $TiO_2$ at pH 5.5 could be attributed to the adsorption of SMT on $TiO_2$, leading to a decrease in the recombination rate and an increase in the quantum efficiency of $TiO_2$ photocatalytic decomposition through the pathway of eqn (6). That is, in the SMT/$TiO_2$ system, the adsorption of SMT on $TiO_2$ may be a key factor controlling the efficiency of electron–hole separation and subsequent SMT photo-decomposition. To further confirm this, the effects of the $TiO_2$ doses on SMT photo-decomposition were evaluated at pH 5.5 with a fixed SMT concentration of 0.072 mM, and the results were shown in Fig. S3.† We did find that provisions of sufficient adsorptive sites of $TiO_2$ indeed enhanced the amounts and the reactive rates of SMT photo-decomposition (Fig. S3† and inserted). For instance, the PFO rate constant ($k_{app}$) of photo-decomposition of 0.072 mM SMT increased from 0.52 to 1.17 $h^{-1}$ with increasing in $TiO_2$ doses from 0.1 to 2.0 g $L^{-1}$ (Table 2). In addition, the mineralization efficiency of SMT was also higher with a greater suspension density of $TiO_2$, *i.e.*, 2.0 g $L^{-1}$ (Fig. S4a†).

Effects of initial SMT concentrations on photo-decomposition of SMT in the presence of 0.5 g $L^{-1}$ $TiO_2$ at pH

Table 2 Pseudo-first-order rate (PFO) rate constants of sulfamethazine (SMT) photo-decomposition in the presence of radical scavengers of isopropanol (ISP) and sodium iodide (NaI) with 0.036–0.162 mM SMT and 0.1–2.0 g $L^{-1}$ $TiO_2$ at pH 5.5

| SMT concentration (mM) | $TiO_2$ loading (g $L^{-1}$) | Scavengers molar ratio (mol $mol^{-1}$) | | PFO rate constant | |
|---|---|---|---|---|---|
| | | ISP[a]/SMT | NaI/SMT | $k_{app}$[b] ($h^{-1}$) | $r^2$ |
| **Initial concentration effect** | | | | | |
| 0.036 | 0.5 | 0 | 0 | 1.61 | 0.99 |
| 0.072 | 0.5 | 0 | 0 | 0.69 | 0.99 |
| 0.162 | 0.5 | 0 | 0 | 0.24 | 0.99 |
| **$TiO_2$ loadings effect** | | | | | |
| 0.072 | 0.1 | 0 | 0 | 0.52 | 0.98 |
| 0.072 | 0.5 | 0 | 0 | 0.69 | 0.99 |
| 0.072 | 2.0 | 0 | 0 | 1.17 | 0.99 |
| **Radical scavengers effect** | | | | | |
| 0.072 | 0.5 | 10 | 0 | 0.32 | 0.99 |
| 0.072 | 0.5 | 100 | 0 | 0.10 | 0.98 |
| 0.072 | 0.5 | 0 | 100 | 0.36 | 0.94 |

[a] ISP indicated the isopropanol. [b] $k_{app}$ represented the rate constant of pseudo-first-order (PFO) model.

5.5 were shown in Fig. S4b.† Although the photo-decomposition rate of SMT decreased with an increase in the initial concentrations of SMT (Fig. S4b,† inserted and Table 2), the amount of photo-induced SMT removal was still higher when a higher concentration of SMT was added. The photo-decomposition kinetics of SMT could also be well described by PFO model, and the $k_{app}$ values of the overall photo-decomposition of SMT were 1.61, 0.69, and 0.24 $h^{-1}$ in a system with the initial SMT concentrations of 0.036, 0.072, and 0.162 mM, respectively (Table 2). Because, the heterogeneous PCDS on $TiO_2$ dominated SMT photo-decomposition and related greatly on the amount of SMT adsorption at pH 5.5, the lack of sufficient adsorption sites on $TiO_2$ may inhibit SMT adsorption and subsequent decomposition.[51]

To distinguish the contributions of major reactive species of holes or OH radicals to SMT photo-decomposition, sodium iodide (NaI) and isopropanol (ISP) were used as the radical scavengers of holes and OH radicals, respectively, during the photo-catalytic reaction.[52,53] As shown in Fig. S5,† in the absence of any radical scavengers (represented by normal system), a highest photo-decomposition of SMT was observed with a $k_{app}$ value of 0.69 $h^{-1}$. After adding the ISP reagent, the PFO rate constant ($k_{app}$) of SMT photo-decomposition decreased from 0.69 to 0.32 $h^{-1}$ with a ISP/SMT molar ratio of 10, and the $k_{app}$ value decreased further to 0.10 $h^{-1}$ when the ISP/SMT molar ratio was increased to 100 (Table 2). Similarly, the $k_{app}$ value decreased from 0.69 to 0.30 $h^{-1}$ with the addition of NaI (*i.e.*, NaI/SMT molar ratio of 100). The decrease in the efficiency of SMT photo-decomposition due to the presence of radical scavenger indicated that the productions of holes and OH radicals on the $TiO_2$ surfaces upon absorbing light energy were responsible for SMT removal (Fig. S5†). However, the ISP may be a more efficient reagent of inhibiting SMT photo-decomposition than NaI because, upon the addition of ISP with a ISP/SMT ratio of 100, the rates of SMT photo-decomposition decreased greatly and closed to that of SMT self-photolysis (Fig. S5†). That is, a complete inhibition of the catalytic oxidation of SMT on $TiO_2$ was observed in a system with an ISP/SMT molar ratio of 100, and thus, the rate constant of SMT photolysis (0.12 $h^{-1}$) was closed to that of $TiO_{2,ISP/SMT=100}$ system (0.10 $h^{-1}$) (Table 2). Because ISP is a major OH radical quencher, the strong inhibition of SMT photo-decomposition with the addition of ISP suggested that OH radicals may be a dominate oxidant for SMT when $TiO_2$ was present.

According to eqn (2), the holes on the $TiO_2$ were the activated sites of producing OH radicals. Upon OH radical productions, they could be adsorbed on $TiO_2$ or be present in solution.[24] Although SMT could be photo-oxidized directly by the holes, the hydrophilic properties of $TiO_2$ surfaces may favor $H_2O$ photolysis on the electron-deficiency sites (*i.e.*, holes), leading to OH radical productions. Thus, we presumed that the adsorbed SMT may be more readily oxidized by the vicinity of adsorbed OH radicals than that by free OH radicals with a short lifetime. Therefore, adsorption of neutral SMT on the surfaces of $TiO_2$ facilitates the photo-catalytic decomposition of SMT.

### 3.3 Intermediates productions during photo-decomposition of SMT

The intermediates (Int.) of the photo-decomposition of SMT were analyzed by HPLC-MS, and the $ESI^+$ and $ESI^-$ fragmentation patterns of intermediates were obtained from the full-scan UV spectra (Fig. S6†). The pathways of SMT photo-decomposition developed at each ESI mode were proposed in Fig. 3. Five intermediates were identified based on the fragmentation patterns of $ESI^+$ which were obtained from the major peaks of chromatograph spectra (Fig. S6†). The SMT parent compound was depicted at a retention time of 15.565 min with a fragment ion at $m/z$ 279 (Fig. S6b†). Two peaks with the retention time of 14.667 and

 

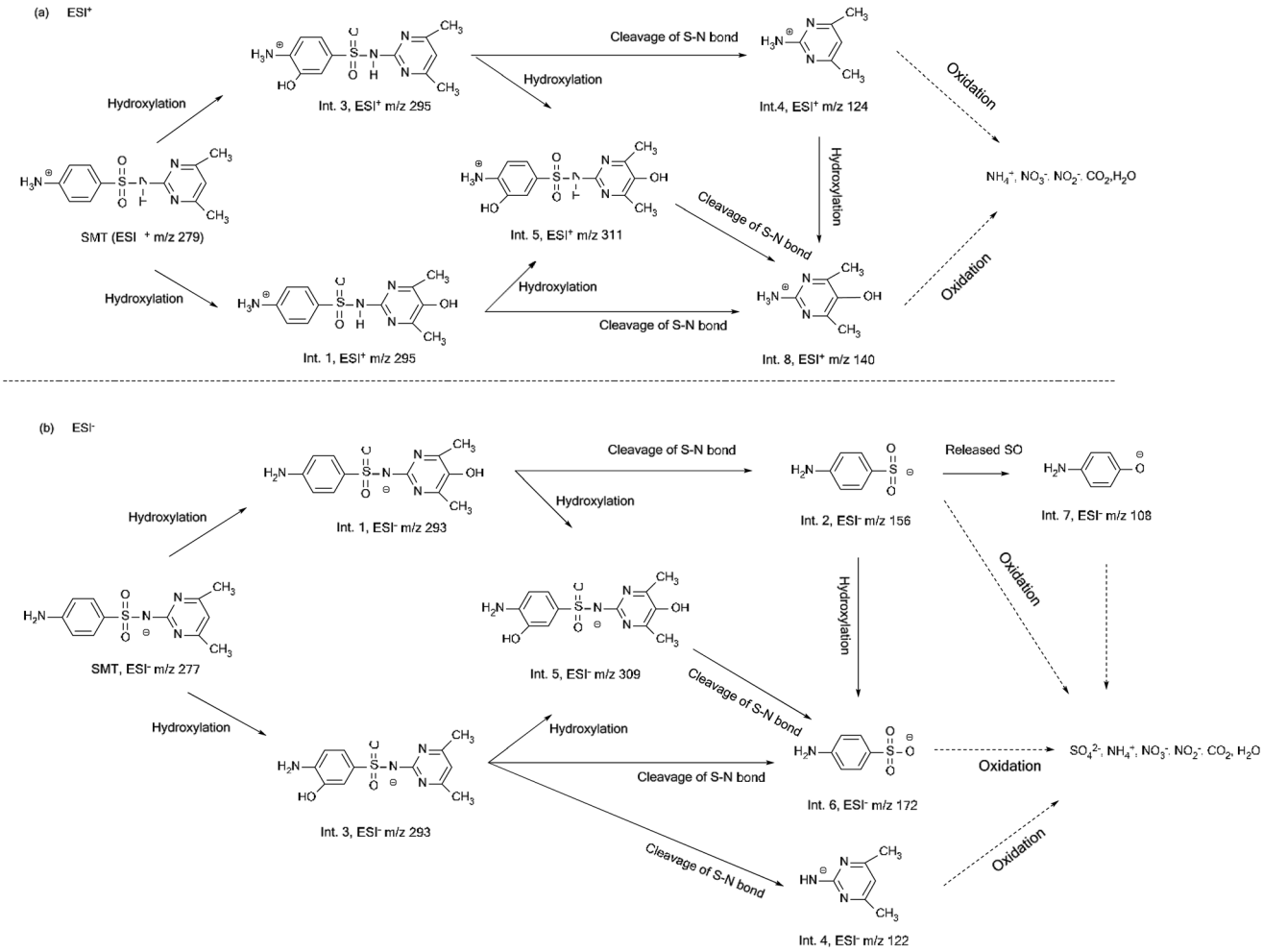


Fig. 3 The possible photo-decomposition pathways of sulfamethazine (SMT) obtained by using (a) $ESI^+$ and (b) $ESI^-$ detection modes.

14.221 min exhibited the same fragment ions at *m*/*z* 295, representing two intermediates of the hydroxylation analogs of SMT (*i.e.*, Int. 1 and Int. 3 in Fig. S6c and d†). The fragment ion of intermediate 5 (*m*/*z* 311) (Fig. S6e†) depicted at the retention time of 13.483 min was attributed to the attachment of hydroxide radical on the benzoic ring and N-heterocyclic moiety of the Int. 1 and Int. 3, respectively (Fig. 3a). A fragment ion at *m*/*z* 124, *i.e.*, intermediate 4, derived from the cleavage of the S–N bond of intermediate 3, was obtained from the peak with a retention time of 12.530 min (Fig. S6f†). The intermediate 8, obtained from the retention time of 4.404 min, possessed a fragment ion at *m*/*z* 140 and was the oxidative product of intermediate 5 or intermediated 1 upon interacting with OH radical (Fig. 3a). The intermediate 8 might be also from the reactions of hydroxylation on the N-heterocyclic moiety of intermediate 4 after the S–N bond of the intermediate 3 was broken (Fig. 3a).

The time-dependent distributions of the intermediates produced from the photo-decomposition of SMT using $ESI^+$ mode were shown in Fig. 4. The fragment ion with a *m*/*z* ratio of 279 ($ESI^+$), representing the SMT parent compound, decreased rapidly over the irradiation time (Fig. 4a). Five intermediates, *i.e.*, Int. 1 (*m*/*z* 295), Int. 3 (*m*/*z* 295), Int. 4 (*m*/*z* 124), Int. 5 (*m*/*z* 311), and Int. 8 (*m*/*z* 140), were detected and their concentrations increased rapidly during the initial 30 min irradiation (Fig. 4b). The productions of maximum concentrations of the intermediates followed the order of Int. 1 > Int. 8 > Int. 4 > Int. 3 > Int. 5 (Fig. 4b). After photo-decomposition of SMT for 1 h, the Int. 1, Int. 3, and Int. 4 decreased significantly, but at the same reaction time the Int. 5 and Int. 8 reached their maximum accumulation concentrations.

Similar to the fragmentation patterns of $ESI^+$, four same intermediates of Int. 1, 3, 4, and 5, with the fragment ions at *m*/*z* 293 (Int. 1 and 3), 122, and 309, respectively, were also found using $ESI^-$ detection mode (Table S1†). The fragment ion with an *m*/*z* ratio of 277 found on $ESI^-$ represented the parent compound of SMT (Fig. S6h†). The fragment ions with *m*/*z* ratios of 156 (Int. 2), 172 (Int. 6), and 108 (Int. 7) were three new intermediates identified by $ESI^-$ upon photo-decomposition of SMT. The fragment ions at *m*/*z* 156 (Int. 2) (Fig. S6i†) was suggested an aniline with a $SO_2$ group derived from the cleavage of the S–N bond of Int. 1 (Fig. 3b). The intermediate 6 was a fragment ion at *m*/*z* 172 (Fig. S6j†), given from the hydroxylation of the intermediate 2 (*m*/*z* 156) or from the cleavages of S–N bond of Int. 3 or Int. 5 (Fig. 3b). The

fragment ion at $m/z$ 108 (Int. 7) (Fig. S6k†) was attributed to the decomposition of Int. 2 and released subsequently SO/$SO_4^{2-}$ (Fig. 3b). Accordingly, the results of mass analyses indicates that the hydroxylation of electrophilic OH radicals on amino-phenol or pyrimidinyl moiety[54,55] played an important role of proceeding subsequently S–N bond and ring cleavage during photo-decomposition of SMT involving $TiO_2$.[56] The mass instrument with $ESI^+$ source was more sensitive to the positively charged groups, and thus, the intermediates with pyrimidinyl group, such as Int. 4 ($m/z$ = 124) and 8 ($m/z$ = 140), were preferentially detected upon photo-decomposition of SMT (Fig. S6†). Although, both positive and negative sources of ESI are suitable detection modes to identify the products of SMT photo-decomposition, the $ESI^-$ source possessed more sensitive response for detecting the acidic products with a sulfate group, *e.g.*, Int. 2, and 6. A similar result was also reported by ref. 31, when analyzed pesticides with carboxyl groups, sulfate, or sulfonate using $ESI^-$.

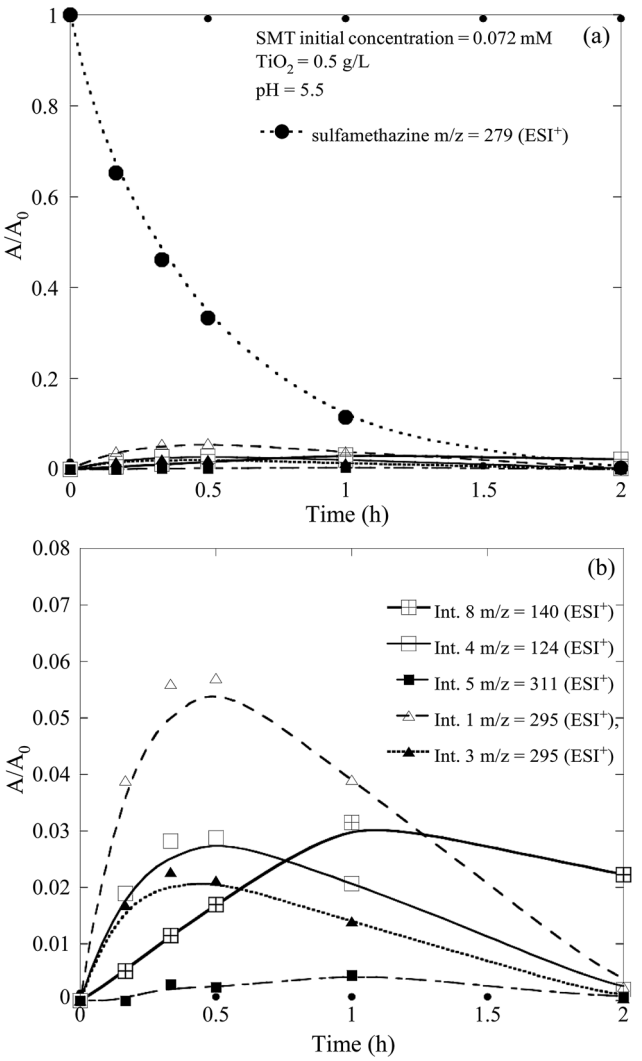


Fig. 4 Time-dependent distributions of (a) 0.072 mM sulfamethazine (SMT) on 0.5 g $L^{-1}$ $TiO_2$ and (b) the major photo-decomposition products of SMT.

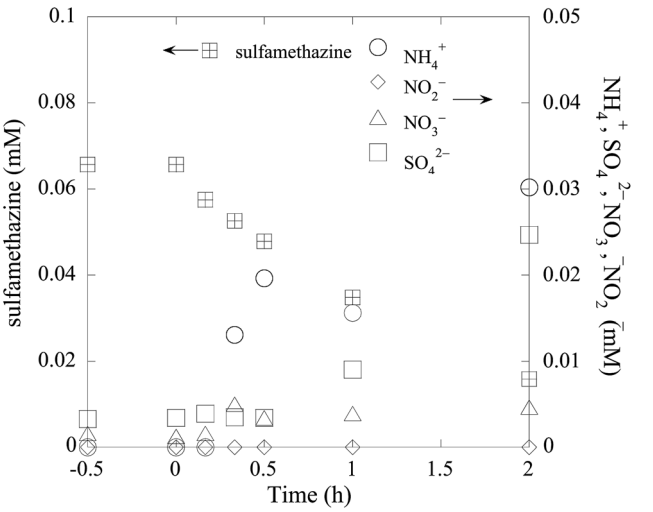


Fig. 5 Productions of the specific ions upon photo-decomposition of 0.072 mM sulfamethazine (SMT) on 0.5 g $L^{-1}$ $TiO_2$.

Upon photo-decomposition of 0.072 mM SMT, about 0.025 and 0.030 mM of $SO_4^{2-}$ and $NH_4^+$, respectively, were detected after 2 h reaction (Fig. 5). However, less than 0.005 mM $NO_3^-$ were detected throughout the photo-decomposition of SMT, and the concentrations of nitrite were lower than the detection limit. As observed previously using a TOC analyzer, about 23.1% of 0.072 mM SMT would be completely mineralized in a system with 0.5 g $L^{-1}$ $TiO_2$ (Fig. S4a†), and thus, the release of S- and N-containing products, such as $SO_4^{2-}$, $NO_3^-$, and $NH_4^+$, were expected after the SMT was completely mineralized, releasing concurrently the oxidative products of $CO_2$ and $H_2O$.[54,57]

### 3.4 Proposed the overall pathway of SMT photo-decomposition

A comprehensive pathway of decomposition of SMT was shown in Fig. 6. Indifferent to the detection modes of using $ESI^+$ or $ESI^-$, the occurrences of hydroxylation on the dimethylpyrimidinyl moiety and aniline portion of SMT, *i.e.*, Int. 1 and 3, respectively, were observed (Fig. 6). Meanwhile, the OH radicals were attached on the vacant hydroxylation positions of Int. 1 or 3, leading to the productions of Int. 5 (Fig. 6). Formations of the Int. 2, 4, 6 and 8 indicated that the cleavages of S–N bond may precede the destruction of the aromatic ring of SMT upon OH radical attack. According to the chromatographic spectra of Fig. S6a,† the intermediates 2, 6, and 7 appeared at about 30 min reaction; however, a significant amount of sulfuric acid was detected after 1 h reaction (Fig. 5). The results demonstrated that the cleavage of S–N bond of SMT occurred before the oxidative released of sulfate ions. Although Yang *et al.*[51] and Yang *et al.*[58] report that sulfate ions could absorb photons, leading to a shortage of photons to activated $TiO_2$ for photo-decomposing pharmaceuticals, the inhibition of SMT decomposition was undiscernible in the study with an accumulation of $SO_4^{2-}$ concentrations up to 0.025 mM. Thus, the kinetic reaction of SMT photo-decomposition on $TiO_2$ was not affected by the reactive products.

 

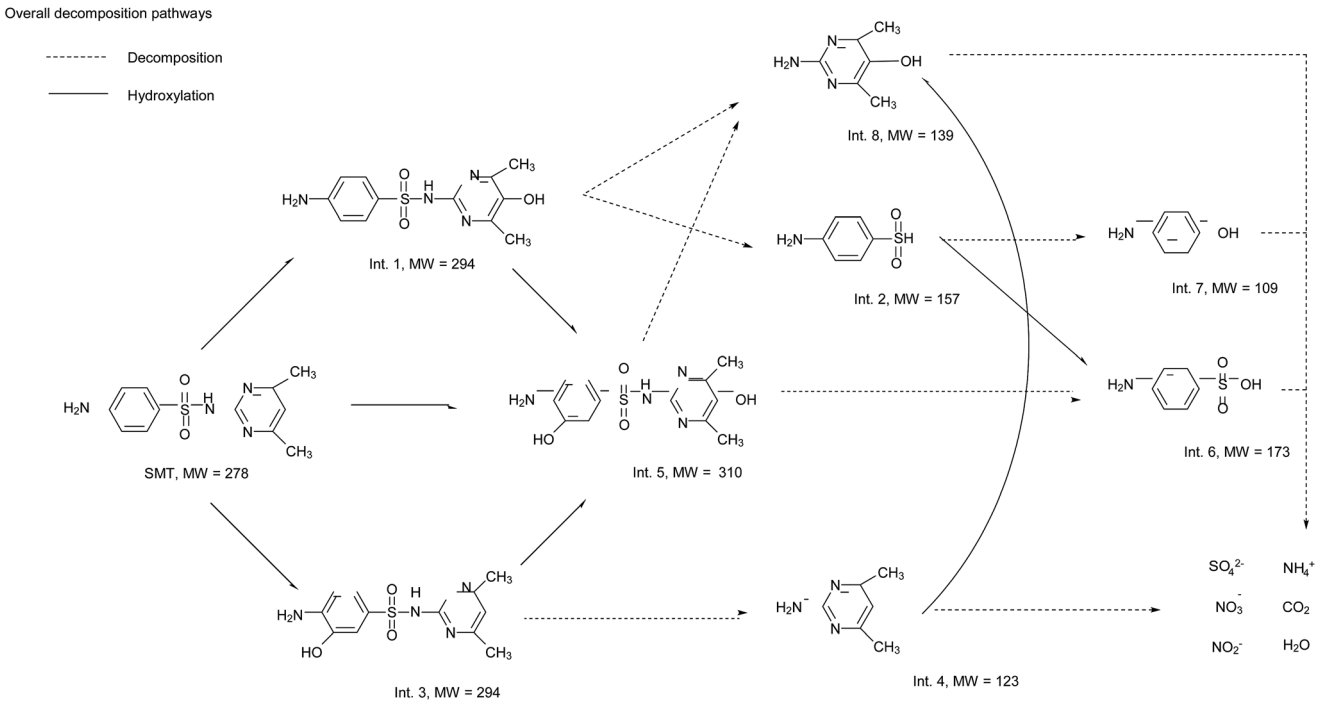


Fig. 6 Proposed the overall pathways of photo-decomposition of sulfamethazine (SMT).

As mentioned previously, the Int. 5 was the hydroxylation products of Int. 1 and 3 on the aniline, and dimethylpyrimidinyl moiety (Int. 4) may be a precursor of Int. 8 because the Int. 4 appeared before Int. 8 (Fig. 4). The Int. 8 with the dimethylpyrimidinyl moiety seemed a more persistent portion of SMT against photo-decompositions because of its rapid accumulation and slow disappearance (Fig. 4). Since the positive ESI mode could not observe fully the intermediates of photo-decomposition of SMT, the negative ESI mode was a compensatory strategy of identifying the aniline portion of SMT. Thus, the identifications of Int. 2, 6, and 7 using the negative ESI mode (Fig. S6†) could help the integral descriptions of the pathways of SMT photo-decomposition. Here, we presumed that the Int. 2, formed by the cleavage of S–N bond of Int. 1, could be the precursor of Int. 6 and 7 (Fig. 6).

Although, based on the changes in the SMT concentrations, SMT could be completely removed in the presence of 0.5 g $L^{-1}$ $TiO_2$ at pH 5.5 under illumination, a complete mineralization of SMT did not occur because approximately 77% of DOC still existed after 2 h reaction (Fig. S4a†). The DOC should be the open-ring products of dimethylpyrimidinyl and aniline, which were not capable of being detected in our current system.

## 4. Conclusion

This study examined the kinetics of photo-decomposition of SMT in the absence and presence of $TiO_2$ at pH 3, 5.5 and 10, and the detail photo-decomposition pathways of SMT were deduced at pH 5.5. Although photolytic reaction dominated SMT decomposition at pH 10, the overall photo-decomposition of SMT was enhanced at pH 5.5 because the SMT adsorption on $TiO_2$ surfaces was greatly increased, promoting the photo-catalytic decomposition of SMT by OH radicals. The photo-decomposition efficiency of SMT increased with increasing $TiO_2$ loading and SMT concentration. During the photo-decomposition of SMT, the results of DOC analyses indicated that SMT was not completely converted to $CO_2$, and the presence of the C-containing intermediates were identified by mass spectra using $ESI^+$ and $ESI^-$ modes. The occurrences of hydroxylations on the benzoic ring and the pyrimidine ring of SMT associated with a direct cleavage the S–N bond on sulfonamide group were suggested to be the major pathways of SMT photo-decomposition. Accompanied with SMT photo-decomposition, a significant increase of inorganic ions, such as $SO_4^{2-}$, was found; however, only trace amount of $NO_3^-$ and $NH_4^+$ was detected. This indicates that N-containing intermediates were more persistent to the photo-decomposition than S-containing products.

## Acknowledgements

The work was financially supported by the Ministry of Science and Technology, ROC under project no. of NSC 101-2621-M-005-005, NSC 102-2621-M-005-001, MOST 103-2621-M-005-002, and MOST 104-2313-B-005-014-MY3, and, in part, by the Ministry of Education, ROC under the Aim for Top University (ATU) plan.

## References

1 J. Wang, T. Zhou, J. Mao and X. Wu, *J. Environ. Chem. Eng.*, 2015, **3**, 2393–2400.
2 C. C. Su, L. M. Bellotindos, A. T. Chang and M. C. Lu, *J. Taiwan Inst. Chem. Eng.*, 2013, **44**, 310–316.

3 Q. Yang, G. Chen, J. Zhang and H. Li, *RSC Adv.*, 2015, **5**, 25541–25549.
4 L. J. Zhou, G. G. Ying, S. Liu, R. Q. Zhang, H. J. Lai, Z. F. Chen and C. G. Pan, *Sci. Total Environ.*, 2013, **444**, 183–195.
5 K.-R. Kim, G. Owens, S.-I. Kwon, K.-H. So, D.-B. Lee and Y. Ok, *Water, Air, Soil Pollut.*, 2011, **214**, 163–174.
6 H. Dolliver and S. Gupta, *J. Environ. Qual.*, 2008, **37**, 1227–1237.
7 J. G. Davis, C. C. Truman, S. C. Kim, J. C. Ascough and K. Carlson, *J. Environ. Qual.*, 2006, **35**, 2250–2260.
8 T. Heberer, *Toxicol. Lett.*, 2002, **131**, 5–17.
9 A. L. Batt, D. D. Snow and D. S. Aga, *Chemosphere*, 2006, **64**, 1963–1971.
10 W. Baran, E. Adamek, J. Ziemiańska and A. Sobczak, *J. Hazard. Mater.*, 2011, **196**, 1–15.
11 M. N. Abellán, B. Bayarri, J. Giménez and J. Costa, *Appl. Catal., B*, 2007, **74**, 233–241.
12 O. González, C. Sans and S. Esplugas, *J. Hazard. Mater.*, 2007, **146**, 459–464.
13 D. Mansour, F. Fourcade, I. Soutrel, D. Hauchard, N. Bellakhal and A. Amrane, *C. R. Chim.*, 2015, **18**, 39–44.
14 D. Mansour, F. Fourcade, I. Soutrel, D. Hauchard, N. Bellakhal and A. Amrane, *J. Taiwan Inst. Chem. Eng.*, 2015, **53**, 58–67.
15 Z. M. Shaykhi and A. A. L. Zinatizadeh, *J. Taiwan Inst. Chem. Eng.*, 2014, **45**, 1717–1726.
16 M. Perez-Moya, M. Graells, G. Castells, J. Amigo, E. Ortega, G. Buhigas, L. M. Perez and H. D. Mansilla, *Water Res.*, 2010, **44**, 2533–2540.
17 S. S. Boxi and S. Paria, *RSC Adv*, 2015, **5**, 37657–37668.
18 P. Wang, T. Zhou, R. Wang and T.-T. Lim, *Water Res.*, 2011, **45**, 5015–5026.
19 Z. Lu, Y. Luo, M. He, P. Huo, T. Chen, W. Shi, Y. Yan, J. Pan, Z. Ma and S. Yang, *RSC Adv*, 2013, **3**, 18373–18382.
20 F. J. Beltrán, A. Aguinaco and J. F. García-Araya, *Water Res.*, 2009, **43**, 1359–1369.
21 W. Baran, E. Adamek, A. Sobczak and A. Makowski, *Appl. Catal., B*, 2009, **90**, 516–525.
22 M. N. Abellán, J. Giménez and S. Esplugas, *Catal. Today*, 2009, **144**, 131–136.
23 A. Carabin, P. Drogui and D. Robert, *J. Taiwan Inst. Chem. Eng.*, 2015, **54**, 109–117.
24 Y. X. Chen, S. Y. Yang, K. Wang and L. P. Lou, *J. Photochem. Photobiol., A*, 2005, **172**, 47–54.
25 L. Hu, P. M. Flanders, P. L. Miller and T. J. Strathmann, *Water Res.*, 2007, **41**, 2612–2626.
26 S. Jiao, S. Zheng, D. Yin, L. Wang and L. Chen, *Chemosphere*, 2008, **73**, 377–382.
27 W. Yang, F. Zheng, X. Xue and Y. Lu, *J. Colloid Interface Sci.*, 2011, **362**, 503–509.
28 M. Kahle and C. Stamm, *Chemosphere*, 2007, **68**, 1224–1231.
29 P. Calza, C. Medana, M. Pazzi, C. Baiocchi and E. Pelizzetti, *Appl. Catal., B*, 2004, **53**, 63–69.
30 Z. R. Wu, W. Q. Gao, M. A. Phelps, D. Wu, D. D. Miller and J. T. Dalton, *Anal. Chem.*, 2004, **76**, 839–847.
31 E. M. Thurman, I. Ferrer and D. Barceló, *Anal. Chem.*, 2001, **73**, 5441–5449.
32 B. Abramović, S. Kler, D. Šojić, M. Laušević, T. Radović and D. Vione, *J. Hazard. Mater.*, 2011, **198**, 123–132.
33 L. L. Ji, W. Chen, S. R. Zheng, Z. Y. Xu and D. Q. Zhu, *Langmuir*, 2009, **25**, 11608–11613.
34 C. Wang, H. Li, S. H. Liao, D. Zhang, M. Wu, B. Pan and B. S. Xing, *Environ. Pollut.*, 2014, **194**, 203–209.
35 M. X. Xie, W. Chen, Z. Y. Xu, S. R. Zheng and D. Q. Zhu, *Environ. Pollut.*, 2014, **186**, 187–194.
36 G. R. Deshpande, B. Rao and N. Someswararao, *Rasayan J. Chem.*, 2009, **2**, 101–107.
37 S. G. Shin, G. Han, J. Lim, C. Lee and S. Hwang, *Water Res.*, 2010, **44**, 4838–4849.
38 X. Huang, Y. Feng, C. Hu, X. Xiao, D. Yu and X. Zou, *Chemosphere*, 2015, **138**, 183–189.
39 M. R. Hoffmann, S. T. Martin, W. Y. Choi and D. W. Bahnemann, *Chem. Rev.*, 1995, **95**, 69–96.
40 Y. He, N. B. Sutton, H. H. H. Rijnaarts and A. A. M. Langenhoff, *Appl. Catal., B*, 2016, **182**, 132–141.
41 D. Friedmann, C. Mendive and D. Bahnemann, *Appl. Catal., B*, 2010, **99**, 398–406.
42 N. Jaffrezicrenault, P. Pichat, A. Foissy and R. Mercier, *J. Phys. Chem.*, 1986, **90**, 2733–2738.
43 M. Teixido, J. J. Pignatello, J. L. Beltran, M. Granados and J. Peccia, *Environ. Sci. Technol.*, 2011, **45**, 10020–10027.
44 H. Sakurai and T. Ishimitsu, *Talanta*, 1980, **27**, 293–298.
45 C. Baeza and D. R. U. Knappe, *Water Res.*, 2011, **45**, 4531–4543.
46 J. K. Challis, J. C. Carlson, K. J. Friesen, M. L. Hanson and C. S. Wong, *J. Photochem. Photobiol., A*, 2013, **262**, 14–21.
47 H. Xiao, G. Liu, Z. Chen and R. Wu, *Journal*, 2015, **1**, 63–67.
48 M. A. Fox and M. T. Dulay, *Chem. Rev.*, 1993, **93**, 341–357.
49 R. M. Alberici and W. F. Jardim, *Appl. Catal., B*, 1997, **14**, 55–68.
50 K. Demeestere, J. Dewulf, B. D. Witte and H. Van Langenhove, *Appl. Catal., B*, 2005, **60**, 93–106.
51 H. Yang, G. Li, T. An, Y. Gao and J. Fu, *Catal. Today*, 2010, **153**, 200–207.
52 C. S. Guo, J. Xu, S. F. Wang, Y. Zhang, Y. He and X. C. Li, *Catal. Sci. Technol.*, 2013, **3**, 1603–1611.
53 K. Ishibashi, A. Fujishima, T. Watanabe and K. Hashimoto, *J. Photochem. Photobiol., A*, 2000, **134**, 139–142.
54 S. Fukahori and T. Fujiwara, *J. Environ. Manage.*, 2015, **157**, 103–110.
55 C. Guo, J. Xu, Y. Zhang and Y. He, *RSC Adv*, 2012, **2**, 4720–4727.
56 S. Fukahori, H. Ichiura, T. Kitaoka and H. Tanaka, *Appl. Catal., B*, 2003, **46**, 453–462.
57 E. Vulliet, C. Emmelin, J.-M. Chovelon, C. Guillard and J.-M. Herrmann, *Appl. Catal., B*, 2002, **38**, 127–137.
58 L. Yang, L. E. Yu and M. B. Ray, *Water Res.*, 2008, **42**, 3480–3488.

 